

Zero-Chirp and Low Power PAM-4 Modulation Based on SOI Cascaded Multimode Interference Structures

Duy Tien LE¹, Ngoc Minh NGUYEN², Trung Thanh LE¹

¹International School (VNU-IS), Vietnam National University (VNU), Hanoi, Vietnam

²Posts and Telecommunications Institute of Technology (PTIT), Hanoi, Vietnam

thanh.le@vnu.edu.vn

Submitted August 8, 2021 / Accepted February 8, 2022

Abstract. *We present a new architecture for generation of multilevel pulse amplitude modulation (PAM-4) signal generation based on cascaded 4×4 multimode interference (MMI) structure used for optical interconnects and data center network. The proposed device can generate two ring resonator structures with capability of critical coupling control. The push-pull configuration then is used at two ring resonators for PAM-4 level generation, so a zero chirp can be achieved. In this structure an M-shape transmission can be created for the first time. We use this property for an extreme reduction of power consumption with a lower level than 4–28 times compared with the PAM-4 generation based on the Mach Zehnder Modulator (MZM), respectively. Based on this structure, an extreme high bandwidth and compact footprint are also achieved. The whole device is designed and analyzed using the existing VLSI (Very-Large Scale Integration) silicon photonics.*

Keywords

Data center networks, high performance computing, multimode interference (MMI), microring resonator, integrated optics, higher order modulation, optical computing systems

1. Introduction

In the literature, on off keying (OOK) modulation is used for the transmitter and receiver architectures in short reach optical links of optical interconnect and data center networks. Recently, configuration of 200 Gb/s and 400 Gb/s systems utilized OOK modulation have been deployed [1]. However, the OOK modulation is limited if the high bandwidth is required. In addition, the complexity of the system increases. As a result, a new efficient higher order modulation is required to avoid complexity. Consequently, various modulation formats with higher spectral efficiency such as discrete multi-tone (DMT), 4-level pulse amplitude modulation (PAM-4) and quadrature phase shift keying (QPSK) have been studied to replace OOK [2].

Multi-level pulse amplitude modulation (PAM-4) is a good candidate for high data rate transmissions with suitable cost and complexity. Compared with other higher modulation such as M-PSK, M-QAM, PAM-4 requires only a limited resource of digital signal processing (DSP) requirements. The PAM-M modulation allows for direct direction of optical intensity signals without requiring complex DSP, although good signal-to-noise ratio is required. PAM-4 has been used for data center and high performance computing systems instead of other modulation methods [3].

In order to generate PAM-4 signal, a significant work has been presented such as silicon photonic microring modulators (MRMs) and travelling-wave Mach-Zehnder modulators (TWMZMs) [4], and segmented electrode MZI [5], vertical-cavity surface-emitting lasers (VCSEL), silicon-germanium electro-optic modulators, silicon hybrid modulators, electro-optic polymer modulators and LiNbO₃ modulators [4]. These approaches require a complex circuit and have low fabrication tolerance. In addition, these structures use directional couplers, so it is very difficult to control the directional coupler to achieve exact coupling ratios. Another limitation of the published approaches is to generate PAM-4 levels with high power consumption due to the requirement of the required phase shifts.

Therefore, in this study, we propose a new architecture to implement a PAM-4 signal generation system by using cascaded 4×4 MMI couplers with the capacity of a zero chirp. Two 4×4 MMI couplers act as two microring resonators with controllable coupling ratios. We control the microring resonator to work in the over coupled-region. Two phase shifters at the ring waveguides are used in the push-pull configuration to obtain the zero chirp parameter. As a result, significant reductions in power consumption can be achieved compared with the conventional MZI architecture. Here we show that bandwidth and fabrication tolerance of the proposed configuration can be achieved, compared to the conventional structure. In addition, silicon photonics is an emerging technology for photonic VLSI systems. Photonic circuits with large scale integrated circuits become feasible and practical with silicon photonics [6]. It uses the CMOS existing technologies so it is com-

patible with CMOS processes. Optical interconnects are the major commercial application of silicon photonics. They are driven by the quickly increasing demand for high-speed optical links in data centers.

2. Design of New PAM-4 Generation Based on 4x4 MMI Cascaded MMIs

Figure 1(a) shows a schematic of the PAM-4 generation architecture based on cascaded 4x4 MMIs. The structure of the phase shifters used for PAM-4 generation and control of the critical coupling for microring resonators are shown in Fig. 1(b). The waveguide structure with the Si core without doping P and N region is shown in Fig. 1(c). In our study, we use a microring resonator with a radius of 15 μm . The waveguide has a width of 500 nm and a height of 220 nm, and it is on a 90 nm slab for a single mode operation [7].

We use two PN junction phase shifters at the push and pull configuration inside a microring resonator waveguide for two bits b_0b_1 , which use the plasma dispersion effect in silicon waveguides as shown in the box of Fig. 1(a). The mode profile of the optical waveguide at 1550 nm is shown in Fig. 1(c), where the effective refractive index is $n_{\text{eff}} = 2.61$ by using the FDM (Finite Difference Method).

The light PN doping concentrations are for reducing the optical scattering loss in the rib waveguide. The widths

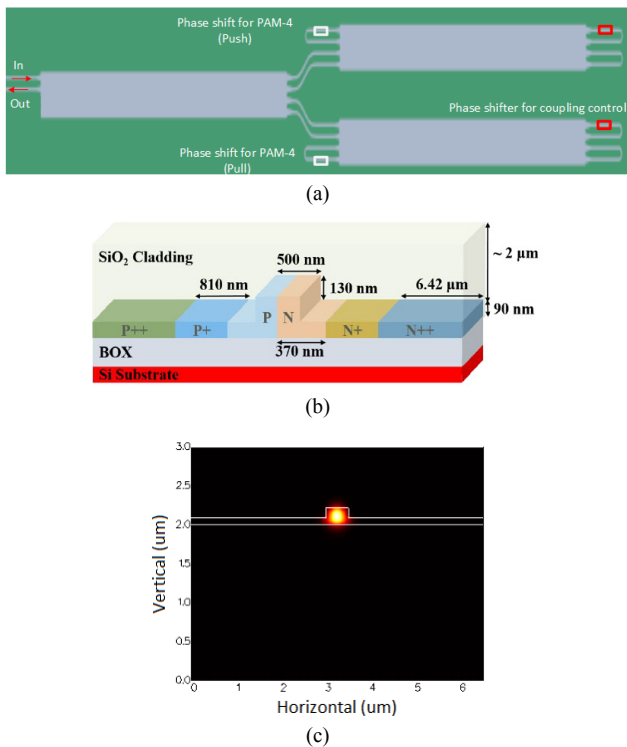


Fig. 1. (a) Scheme of a PAM-4 signal generation based on cascaded 4x4 MMI couplers. (b) Cross-sectional view of the phase shifter. (c) Fundamental mode of the single mode SOI rib waveguide.

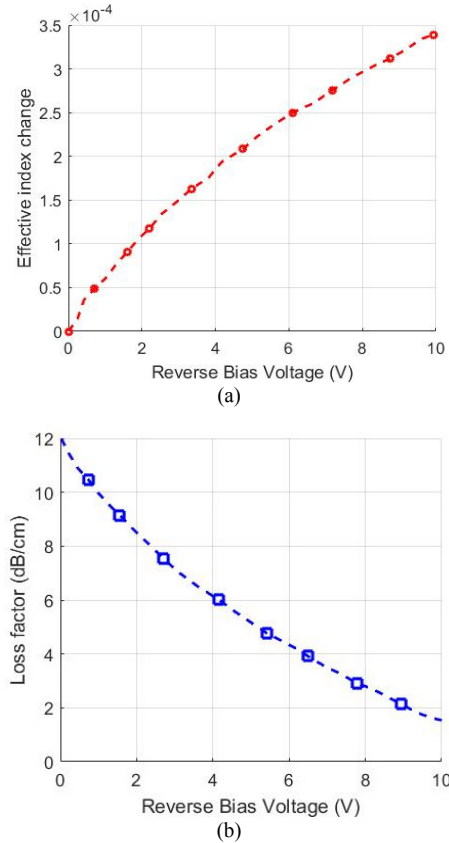


Fig. 2. (a) Effective index change and (b) loss factor at different bias voltage at the PN junction.

of the P doped layer and N doped layer in the 90 nm slab waveguide are both 1 μm . There are also P⁺⁺ and N⁺⁺ doped regions with a width of 6.35 μm , which are designed for ohmic contact with the metal pads. They are both 1 μm away from the edge of the rib waveguide. The simulated peak doping concentrations in are $7.8 \times 10^{17} \text{ cm}^{-3}$ for P, $2.1 \times 10^{18} \text{ cm}^{-3}$ for N, $3.9 \times 10^{19} \text{ cm}^{-3}$ for P⁺⁺ and $9.7 \times 10^{19} \text{ cm}^{-3}$ for N⁺⁺ [8]. The change in index of refraction is phenomenon logically described by Soref and Bennett model [9]. Here we focus on the central operating wavelength of around 1550 nm. The change in refractive index is $\Delta n(\text{at } 1550 \text{ nm}) = -8.8 \times 10^{-22} \Delta N - 8.5 \times 10^{-18} \Delta P^{0.8}$ and the change in absorption is described by $\Delta \alpha(\text{at } 1550 \text{ nm}) = 8.5 \times 10^{-18} \Delta N + 6 \times 10^{-18} \Delta P [\text{cm}^{-1}]$; ΔN and ΔP are the electron concentration change and the hole concentration change (cm^{-3}). Figure 2 plots the simulated effective index changes and the propagation losses when applying reverse bias voltages on the four PN junction designs in Fig. 1(b).

By a proper selection of width, length and positions of the input waveguides for a 2x4 MMI coupler in Fig. 1(a) at the position in x-axis $x_i = (i + \frac{1}{2}) W_{\text{MMI}}/N$ ($i = 0, 1, 2, 3$), W_{MMI} is the width of the MMI coupler. We can find a 2x4 MMI structure to achieve a special characteristic [10]. By using the mode propagation method, the width and length of the MMI coupler are 6 μm and 225 μm , respectively [11]. Figure 3 presents the field propagation through the 2x4 MMI coupler at the optimal length for input signal at port 1.

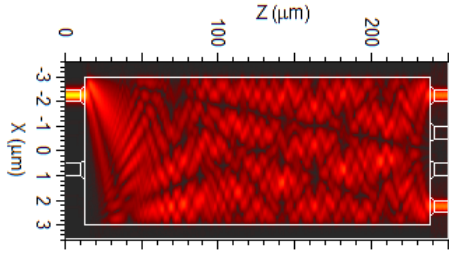


Fig. 3. Field propagation through the 2×4 MMI coupler at the optimal width and length.

We showed that the characteristics of an MMI device is described by a transfer matrix [11]. This transfer matrix is a very useful tool for analysing cascaded MMI structures. The phase ϕ_j associated with imaging an input i to an output j in an MMI coupler. These phases ϕ_j form a matrix $\mathbf{S}_{4 \times 4}$, with i representing the row number, and j representing the column number [12]. A single 4×4 MMI coupler at a length of $L_{\text{MMI}} = 3L_\pi/2$, where L_π is the beat length of the MMI, is described by the following transfer matrix [13]:

$$\mathbf{S}_{4 \times 4 \text{MMI}} = \frac{1}{2} \begin{bmatrix} 1-j & 0 & 0 & 1+j \\ 0 & 1-j & 1+j & 0 \\ 0 & 1+j & 1-j & 0 \\ 1+j & 0 & 0 & 1-j \end{bmatrix}. \quad (1)$$

The output and input amplitudes at 4 ports of the 4×4 multimode waveguide can be expressed by

$$\overline{\mathbf{E}}_{\text{out}} = \begin{pmatrix} E_{\text{out},1} \\ E_{\text{out},2} \\ E_{\text{out},3} \\ E_{\text{out},4} \end{pmatrix} = \mathbf{S}_{4 \times 4} \begin{pmatrix} E_{\text{in},1} \\ E_{\text{in},2} \\ E_{\text{in},3} \\ E_{\text{in},4} \end{pmatrix} = \mathbf{S}_{4 \times 4} \overline{\mathbf{E}}_{\text{in}} \quad (2)$$

where $E_{\text{in},i}$ ($i = 1, 2, 3, 4$) and $E_{\text{out},j}$ ($j = 1, 2, 3, 4$) are complex amplitudes at input ports and output ports 1–4, respectively. From (1) and (2), we can calculate the relationships between the input and output amplitudes of Fig. 1 as follows:

$$\begin{pmatrix} E_{\text{in},1} \\ E_{\text{in},4} \end{pmatrix} = \mathbf{M} \begin{pmatrix} E_{\text{in},2} \\ E_{\text{in},3} \end{pmatrix} = e^{j\frac{\Delta\varphi}{2}} \begin{bmatrix} \tau & \kappa \\ \kappa^* & -\tau^* \end{bmatrix} \begin{pmatrix} E_{\text{in},2} \\ E_{\text{in},3} \end{pmatrix} \quad (3)$$

where $\mathbf{M} = e^{j\frac{\Delta\varphi}{2}} \begin{bmatrix} \tau & \kappa \\ \kappa^* & -\tau^* \end{bmatrix}$, $\tau = \cos\left(\frac{\Delta\varphi}{2}\right)$, $\kappa = \sin\left(\frac{\Delta\varphi}{2}\right)$

are coupling ratios of the microring resonator. The phase shift $\Delta\varphi$ is induced by the PN junction and can be calculated by [14]:

$$\Delta\varphi = \frac{2L_{\text{PS}}}{\lambda} \Delta n_{\text{eff}}(V) \quad (4)$$

where L_{PS} is the length of the phase shifter and $\Delta n_{\text{eff}}(V)$ is the change of effective index on the applied voltage.

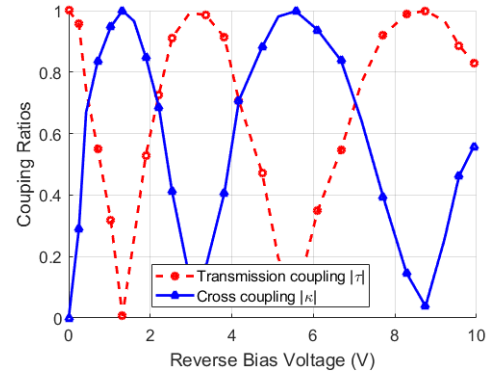


Fig. 4. Control of the microring resonator coupling ratio based on the PN phase shifter.

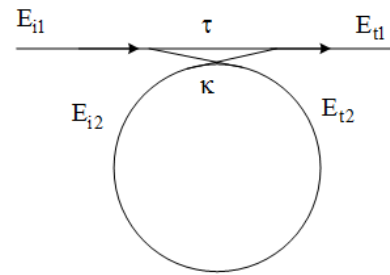


Fig. 5. 4×4 MMI coupler with feedback waveguide working as a microring resonator.

As a result, the coupling ratios of the microring resonator based on 4×4 MMI coupler in Fig. 1(a) can be controlled by the phase shifter as shown in Fig. 4.

The 4×4 MMI couplers with feedback waveguides work as two microring resonators shown in Fig. 5 [12]. Here we use two identical microring resonators. This means that the coupling ratio, loss factor and radius are the same.

For a microring resonator, the field at the output of the microring resonator is expressed by using the Yariv's model [15]:

$$\begin{pmatrix} E_{t1} \\ E_{t2} \end{pmatrix} = \begin{pmatrix} \tau & \kappa \\ -\kappa^* & \tau \end{pmatrix} \begin{pmatrix} E_{i1} \\ E_{i2} \end{pmatrix} \quad (5)$$

where κ and τ are the cross coupling and transmission coupling coefficients of the couplers (two identical couplers for two microring resonators); $E_{i1}, E_{i2}, E_{t1}, E_{t2}$ are the complex amplitudes of the input and output signals in Fig. 5; $E_{i2} = \alpha \exp(j\phi) E_{i2}$, $\phi_1 = -\phi_2 = \phi$ is the phase shift inside the microring resonator, including the phase shift due to optical waveguide $\phi_0 = 4\pi^2 n_{\text{eff}} R / \lambda$ and α is the loss factor of the field after one round trip through the microring resonator; n_{eff} is the effective index and L_R is the microring resonator length.

The output field and input field of a single microring resonator is:

$$E_{t1} = E_{i1} \frac{-\alpha + \tau e^{-j\phi}}{-\alpha \tau^* + e^{-j\phi}}. \quad (6)$$

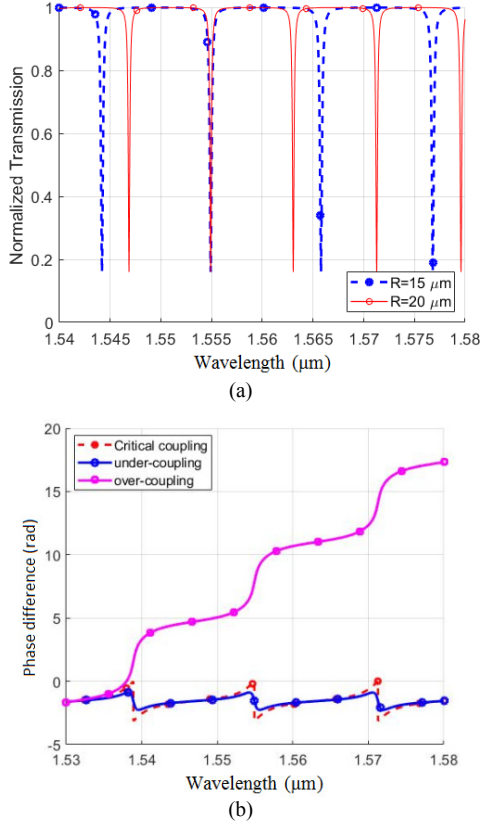


Fig. 6. (a) Transmissions and (b) phase shift for different cases of the single microring resonator working at critical coupling, under-coupling and over-coupling condition.

In order to accumulate the phase shift of single microring resonator into the overall transmission of the device, we carefully design both microring resonators working at the over-coupled condition [16]. The transmissions of the device and phase shifts of the microring resonators with radii of 15 and 16 μm are shown in Fig. 6 for three coupling conditions.

In Fig. 1(a), by applying binary non-return-to-zero (NRZ) electrical signal with voltage levels V_0, V_1, V_2, V_3 to the phase shifter in push-pull configuration, data bits 00, 01, 10, 11 are obtained in the output power. Modelling can be used to find out the voltages required to reach 4 equally spaced power levels, while exploiting the full dynamic range of the output transmission:

$$E_{\text{out}} = \frac{1}{2} E_{\text{in}} \left(\frac{-\alpha + \tau e^{-j\phi}}{-\alpha\tau^* + e^{-j\phi}} + \frac{-\alpha + \tau e^{-j\phi_2}}{-\alpha\tau^* + e^{-j\phi_2}} \right). \quad (7)$$

We apply data signal levels 0, 1, 2, 3 on the phase shift of the 4×4 MMI coupler 1, the inverted data levels 3, 2, 1, 0 are applied on the phase shift of the 4×4 MMI coupler 2 simultaneously to achieve the push-pull operation of the device. The chirp of the modulator is estimated by the chirp parameter [17]

$$CP = 2I \left(\frac{\partial \phi_{\text{total}}}{\partial t} \right) / \left(\frac{\partial I}{\partial t} \right) = 2I \left(\frac{\partial \phi_{\text{total}}}{\partial V} \right) / \left(\frac{\partial I}{\partial V} \right) \quad (8)$$

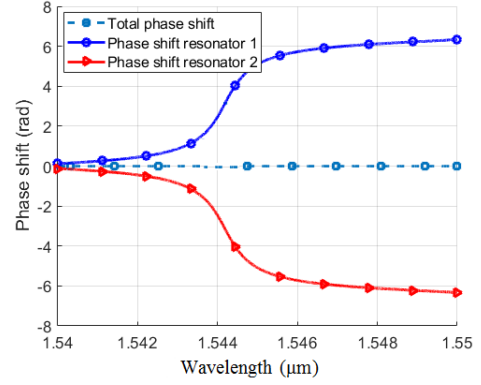


Fig. 7. Phase response of the proposed device with zero chirp.

where V is the applied voltage, ϕ_{total} is the total phase in the structure, I is the modulated optical intensity, both are the functions of time t .

Figure 7 shows the phase response of the proposed device. The simulations show that the phases are all zero, no matter what input data value that is applied. As a result, the proposed device is capable of zero-chirp modulation.

Figure 8 shows the simulations of the normalized transmissions of the proposed device compared with the MZM structure. By controlling the coupling coefficient ratio to device work at the overcoupled region, we can achieve a small power to obtain the desired levels of PAM-4 and the M-shape transmission can be achieved.

In order to compare the power consumption with the conventional MZI structure, we compare the results based M-shape presented in this research with the conventional Mach-Zehnder Modulator (MZM). This result shows that the power consumption to achieve multilevel PAM-4 is extremely low compared with the MZM based PAM-4 generation, but it provides a higher bandwidth and large fabrication tolerance compared with conventional structure based on the MZM in the literature. The simulation results are shown for data bits 00, 01, 11, 10, the phase shift for push-pull configuration in Fig. 1(a) must be $0.08\pi, 0.12\pi, 0.16\pi$ and 0.21π (rad), respectively. In order to achieve a linear region, four normalized output powers at 0.2, 0.4, 0.6 and 0.8 are selected.

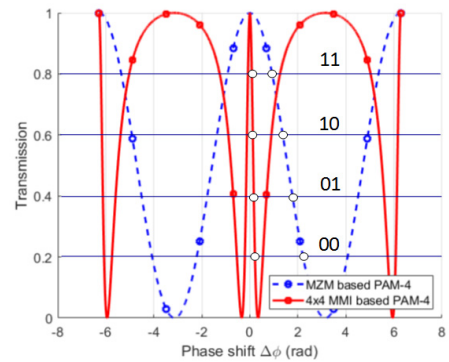


Fig. 8. Comparison of the MZM and the proposed PAM-4 generation architecture in this paper.

| Bit | Required voltages for PAM-4 levels | Phase shifts required for the MZM | Phase shifts at the resonator 1 (Push) | Phase shifts at the resonator 2 (Pull) |
|-----|------------------------------------|-----------------------------------|--|--|
| 00 | V0 (0.2) | 2.23 rad | 0.08 rad | 0.21 rad |
| 01 | V1 (0.4) | 1.77 rad | 0.12 rad | 0.16 rad |
| 10 | V2 (0.6) | 1.37 rad | 0.16 rad | 0.12 rad |
| 11 | V3 (0.8) | 0.92 rad | 0.21 rad | 0.08 rad |

Tab. 1. PAM-4 levels based on two segmented phase shifters.

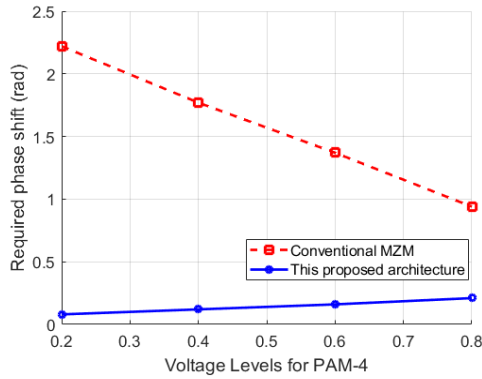


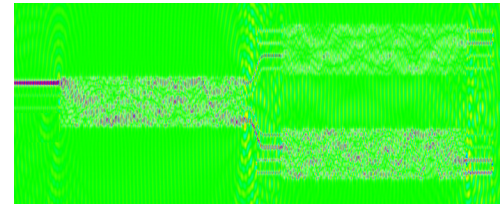
Fig. 9. Phase shifts required for PAM-4 levels (normalization).

The required phase shifts to achieve four levels of PAM-4 signal are shown in Tab. 1 and Fig. 9. From this simulation, we see that the transmission of the proposed architecture has a great linearity. Figure 9 shows the required phase shifts to obtain four PAM-4 levels when using the proposed structure and the conventional MZM. The phase shift is reduced from 4 to 28 times with four PAM-4 levels respectively, compared with the phase shift required when the MZM is used.

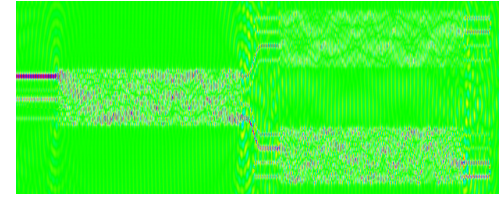
The FDTD simulation of the whole device is shown in Fig. 10 when the four levels of PAM-4, respectively 00, 01, 10 and 11 injected into the segmented phase shifters, respectively. In our FDTD simulations, a Gaussian light pulse of 15 fs pulse width is launched from the input to investigate the transmission characteristics of the device. The grid sizes used in our FDTD are $\Delta x = \Delta y = 5$ nm and $\Delta z = 10$ nm. The waveguide parameters are the ring radius of 15 μm , single mode waveguide width of 500 nm and height of 220 nm. The simulations show that there is a good agreement between the theoretical predictions and FDTD simulations. The normalized power levels at the output are about 0.2, 0.4, 0.6 and 0.8, respectively. For this structure, the laser input and receiver can be designed at the same side. This is particularly suitable for integrated circuit applications.

3. Conclusion

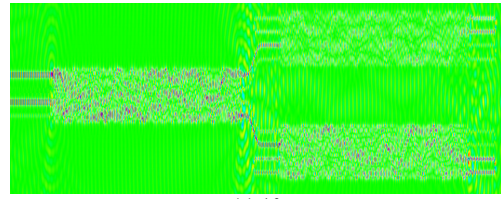
We have proposed a new approach for PAM-4 signaling implementation using cascaded 4×4 MMI couplers based on CMOS technology. The push-pull configuration is used at two ring resonators for PAM-4 level generation,



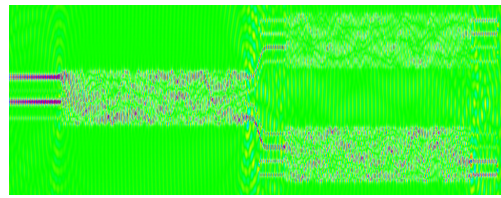
(a) 00



(b) 01



(c) 10



(d) 11

Fig. 10. FDTD simulation of the whole device when input signal is at port 1.

so a zero chirp can be achieved. The structure can create a Fano like shape and we use this property for an extreme reduction of power consumption with a lower level than 4–28 times compared with the PAM-4 generation based on the Mach Zehnder Modulator (MZM), respectively. Based on this structure, an extreme high bandwidth and compact footprint are also achieved. The whole device is designed and analyzed using the existing VLSI silicon photonics. The approach is also suitable and useful for high performance computing, multicore and high speed data center systems.

Acknowledgments

This research is funded by the Vietnam National Foundation for Science and Technology Development (NAFOSTED) under grant number 103.03-2018.354.

References

- [1] XIE, C., SPIGA, S., DONG, P., et al. 400-Gb/s PDM-4PAM WDM system using a monolithic 2×4 VCSEL array and coherent

- detection. *Journal of Lightwave Technology*, 2015, vol. 33, no. 3, p. 670–677. DOI: 10.1109/JLT.2014.2363017
- [2] WANG, K., KONG, M., ZHOU, W., et al. 200-Gbit/s PAM4 generation by a dual-polarization Mach-Zehnder modulator without DAC. *IEEE Photonics Technology Letters*, 2020, vol. 32, no. 18, p. 1223–1226. DOI: 10.1109/LPT.2020.3017535
- [3] BINH, L. N. *Optical Modulation: Advanced Techniques and Applications in Transmission Systems and Networks*. CRC Press, 2019. ISBN: 9780367875046
- [4] SHI, W., XU, Y., SEPEHRAN, H., et al. Silicon photonic modulators for PAM transmissions. *Journal of Optics*, 2018, vol. 20, no. 8, p. 1–18. DOI: 10.1088/2040-8986/aacd65
- [5] KIM, M., KWON, D. H., RHO, D. W., et al. A low-power 28-Gb/s PAM-4MZM driver with level pre-distortion. *IEEE Transactions on Circuits and Systems II: Express Briefs*, 2021, vol. 68, no. 3, p. 908–912. DOI: 10.1109/TCSII.2020.3020128
- [6] TZINTZAROV, G. N., RAO, S. G., CRESSLER, J. D. Integrated silicon photonics for enabling next-generation space systems. *Photonics*, 2021, vol. 8, no. 4, p. 1–20. DOI: 10.3390/photonics8040131
- [7] LI, R., PATEL, D., EL-FIKY, E., et al. High-speed low-chirp PAM-4 transmission based on push-pull silicon photonic microring modulators. *Optics Express*, 2017, vol. 25, no. 12, p. 13222–13229. DOI: 10.1364/oe.25.013222
- [8] SAMANI, A., VEERASUBRAMANIAN, V., EL-FIKY, E., et al. A silicon photonic PAM-4 modulator based on dual-parallel Mach-Zehnder interferometers. *IEEE Photonics Journal*, 2016, vol. 8, no. 1, p. 1–10. DOI: 10.1109/jphot.2015.2512105
- [9] EMELETT, S. J., R. SOREF, R. Design and simulation of silicon microring optical routing switches. *IEEE Journal of Lightwave Technology*, 2005, vol. 23, no. 4, p. 1800–1808. DOI: 10.1109/JLT.2005.844494
- [10] LE, T. T. Two-channel highly sensitive sensors based on 4×4 multimode interference couplers. *Photonic Sensors*, 2017, vol. 7, no. 4, p. 357–364. DOI: 10.1007/s13320-017-0441-1
- [11] LE, T. T. *Multimode Interference Structures for Photonic Signal Processing: Modeling and Design*. Germany: Lambert Academic Publishing, May 2010. ISBN: 978-3838361192
- [12] LE, T. T., CAHILL, L. Generation of two Fano resonances using 4×4 multimode interference structures on silicon waveguides. *Optics Communications*, 2013, vol. 301–302, p. 100–105. DOI: 10.1016/j.optcom.2013.03.051
- [13] LE, T. T., CAHILL, L. The design of 4×4 multimode interference coupler based microring resonators on an SOI platform. *Journal of Telecommunications and Information Technology*, 2009, no. 2, p. 58–62. ISSN: 1509-4553
- [14] LE, T. T., LE, D.-T. High FSR and critical coupling control of microring resonator based on graphene-silicon multimode waveguides. In Steglich, P. (Ed.) *Electromagnetic Propagation and Waveguides in Photonics and Microwave Engineering*. IntechOpen, 2020. DOI: 10.5772/intechopen.92210
- [15] YARIV, A. Universal relations for coupling of optical power between microresonators and dielectric waveguides. *Electronics Letters*, 2000, vol. 36, no. 4, p. 321–322. DOI: 10.1049/el:20000340
- [16] LE, D.-T., NGUYEN, M.-C., LE, T. T. Fast and slow light enhancement using cascaded microring resonators with the Sagnac reflector. *Optik - International Journal for Light and Electron Optics*, 2017, vol. 131, p. 292–301. DOI: 10.1016/j.ijleo.2016.11.038
- [17] KOYAMA, F., IGA, K. Frequency chirping in external modulators. *Journal of Lightwave Technology*, 1988, vol. 6, no. 1, p. 87–93. DOI: 10.1109/50.3969